CANCER

A dominant-negative effect drives selection of *TP53* missense mutations in myeloid malignancies

**Steffen Boettcher[1,2,3], Peter G. Miller[1,2,3], Rohan Sharma[2,3], Marie McConkey[2,3], Matthew Leventhal[2,3], Andrei V. Krivtsov[4], Andrew O. Giacomelli[1,2,5], Waihay Wong[2,3], Jesi Kim[3], Sherry Chao[2,6], Kari J. Kurppa[1,7], Xiaoping Yang[2], Kirsten Milenkowic[2], Federica Piccioni[2], David E. Root[2], Frank G. Rücker[8], Yael Flamand[9], Donna Neuberg[9], R. Coleman Lindsley[1,2], Pasi A. Jänne[1,7], William C. Hahn[1,2], Tyler Jacks[10,11,12], Hartmut Döhner[8], Scott A. Armstrong[4], Benjamin L. Ebert[1,2,3,13]*

TP53, which encodes the tumor suppressor p53, is the most frequently mutated gene in human cancer. The selective pressures shaping its mutational spectrum, dominated by missense mutations, are enigmatic, and neomorphic gain-of-function (GOF) activities have been implicated. We used CRISPR-Cas9 to generate isogenic human leukemia cell lines of the most common *TP53* missense mutations. Functional, DNA-binding, and transcriptional analyses revealed loss of function but no GOF effects. Comprehensive mutational scanning of p53 single–amino acid variants demonstrated that missense variants in the DNA-binding domain exert a dominant-negative effect (DNE). In mice, the DNE of p53 missense variants confers a selective advantage to hematopoietic cells on DNA damage. Analysis of clinical outcomes in patients with acute myeloid leukemia showed no evidence of GOF for *TP53* missense mutations. Thus, a DNE is the primary unit of selection for *TP53* missense mutations in myeloid malignancies.

The transcription factor p53, encoded by its gene *TP53*, is a tumor suppressor involved in the response to pathogenic stimuli such as DNA damage, oxidative stress, and oncogenic hyperproliferation (*1*). *TP53* is the most frequently mutated gene in human cancer. *TP53*-mutant acute myeloid leukemia (AML) and myelodysplastic syndromes (MDS) have an extremely poor prognosis (*2*), are often refractory to chemotherapy (*3*), and have a high rate of relapse after allogeneic hematopoietic stem cell transplantation (*4*).

About 80% of mutations in *TP53* across all cancer subtypes are protein-altering missense mutations that occur in the DNA-binding domain, clustering at several hotspot amino acid residues (*5*). Loss of heterozygosity is a common but not mandatory event during clonal evolution of tumors with *TP53* missense mutations (*6*). This unusual mutational spectrum for a tumor suppressor gene, which normally undergoes biallelic inactivation, has led to the hypothesis that p53 missense mutants may be selected for because of an oncogenic gain of function (GOF) (*7*, *8*). Supporting evidence comes from in vitro and in vivo studies in mice that have demonstrated higher oncogenic potential of $p53^{missense}$ tumors compared with $p53^{null}$ tumors (*9*, *10*). Mutant p53 has been shown to engage in neomorphic protein-protein interactions with other transcription factors, resulting in abnormal tumor-promoting transcriptional programs (*11*–*15*). An alternative hypothesis is that selection for *TP53* missense mutations may be due to a dominant-negative effect (DNE), leading to nonmutational impairment of the remaining wild-type allele (*16*–*19*). Although mutant p53 pathophysiology has largely been studied in epithelial cancers, with a focus on solid tumor phenotypes, such as migration, invasion, and metastasis, the effects of *TP53* missense mutations in the hematopoietic system have been investigated less thoroughly. The selective forces shaping the mutational spectrum of *TP53* in myeloid malignancies have remained elusive but may be relevant for rational design of therapies aimed at preventing clonal selection of *TP53*-mutant clones. We sought to elucidate the functional consequences of *TP53* missense mutations in myeloid malignancies using a series of isogenic cellular models facilitated by advances in genome editing that enable systematic examination of mutant alleles.

We identified the six most frequent *TP53* missense mutations (fig. S1) in the largest cohort of high-risk patients with MDS analyzed to date (*4*) and introduced these mutations, along with null alleles, into two independent human AML cell line models using CRISPR-Cas9 genome editing (Fig. 1A and figs. S2A and S3A). These isogenic cell lines allow comparison of mutant, wild-type, and null alleles expressed from the endogenous locus, leaving the full complexity of p53 feedback mechanisms intact. We generated K562-*TP53* isogenic cells by repairing the hemizygous $TP53^{Q136fs}$ mutation in parental K562, which reactivated wild-type p53 activity in the K562 cells, and then introducing *TP53* missense and null mutations (fig. S2, A to C, and table S1). In the AML cell line MOLM13 that carries two wild-type *TP53* copies, missense and null mutations were introduced into one or both endogenous loci (fig. S3A and table S2).

We characterized these isogenic cell lines with allelic series of *TP53* genotypes in various functional assays. Assessment of cell cycle status and apoptosis after DNA damage revealed intact functionality of these p53-regulated pathways in wild-type *TP53* K562 and MOLM13 isogenic cells (Fig. 1B and figs. S2D and S3B) with the exception of a previously described (*20*) intrinsic apoptotic defect in parental K562 cells (fig. S2, E and F). *TP53*-mutant MOLM13 isogenic cells were relatively resistant to apoptosis (Fig. 1B), and both *TP53*-mutant MOLM13 and K562 isogenic cells failed to arrest in G1 (figs. S2D and S3B). In both isogenic cell line models, the abundance of p53 protein, in steady-state and on daunorubicin-induced DNA damage, was influenced by specific mutations (Fig. 1C and fig. S2G). Furthermore, in contrast with previous studies in which overexpression of wild-type p53 in $TP53^{null}$ cancer cell lines resulted in decreased proliferation (*21*–*23*), expression of wild-type or mutant p53 from the endogenous locus did not affect cell proliferation under steady-state conditions in either cell line model (Fig. 1D and fig. S2H).

MOLM13-*TP53* cells with either missense or null alleles were equally resistant to daunorubicin-induced apoptosis (Fig. 1B), and accordingly, both $TP53^{missense/-}$ and $TP53^{-/-}$ cells were equally more resistant to chemotherapeutics than $TP53^{+/+}$ cells (Fig. 1E). This translated into a sustained competitive advantage over $TP53^{+/+}$ cells, as determined by in vitro mixing experiments (fig. S4, A to C). Consequently, no competitive fitness difference was observed when *TP53* missense mutant cells were cocultured with *TP53* null cells in the presence of dimethyl sulfoxide (DMSO) or daunorubicin (fig. S5, A to C). The slight increase in percentage of $TP53^{Y220C/-}$ and $TP53^{M237I/-}$ cells relative to $TP53^{-/-}$ cells in MOLM13 isogenic cells (fig. S5B) but not K562 isogenic cells (fig. S5C) was therefore considered to be due to subtle differences in proliferative capacities between isogenic MOLM13 lines.

[1]Department of Medical Oncology, Dana-Farber Cancer Institute, Boston, MA 02215, USA. [2]Broad Institute of Massachusetts Institute of Technology and Harvard University, Cambridge, MA 02142, USA. [3]Division of Hematology, Brigham and Women's Hospital, Harvard Medical School, Boston, MA 02115, USA. [4]Department of Pediatric Oncology, Dana-Farber Cancer Institute, Boston, MA 02215, USA. [5]The Campbell Family Institute for Breast Cancer Research, Princess Margaret Cancer Centre, University Health Network, Toronto, ON M5G 2M9, Canada. [6]Department of Biomedical Informatics, Harvard University, Boston, MA 02115, USA. [7]Belfer Center for Applied Cancer Science, Dana-Farber Cancer Institute, Boston, MA 02215, USA. [8]Department of Internal Medicine III, University of Ulm, 89081 Ulm, Germany. [9]Department of Biostatistics and Computational Biology, Dana-Farber Cancer Institute, Boston, MA 02215, USA. [10]David H. Koch Institute for Integrative Cancer Research, Massachusetts Institute of Technology, Cambridge, MA 02139, USA. [11]Department of Biology, Massachusetts Institute of Technology, Cambridge, MA 02139, USA. [12]Howard Hughes Medical Institute, Massachusetts Institute of Technology, Cambridge, MA 02139, USA. [13]Howard Hughes Medical Institute, Dana-Farber Cancer Institute, Boston, MA 02215, USA.
*Corresponding author. Email: benjamin_ebert@dfci.harvard.edu

Collectively, *TP53* isogenic AML cell lines generated by CRISPR-Cas9 genome editing not only faithfully recapitulate p53 biology but also reveal that cells with *TP53* missense and null alleles show the same oncogenic phenotypes in vitro with respect to proliferative capacity, decreased apoptotic potential, lack of G_1 cell cycle arrest, and resistance to cytotoxic agents.

The vast majority of *TP53* missense mutations affect p53's DNA-binding domain, which raises the possibility that they result in activation of de novo transcriptional programs. We therefore performed chromatin immunoprecipitation sequencing (ChIP-seq) and RNA-seq analyses in both isogenic cell line models in steady state and after DNA damage. First, we determined enrichment of wild-type or missense mutant p53 binding relative to the p53 null state, which served as the control. As expected, we observed strong enrichment of wild-type p53 binding to promoter regions in both DMSO- and daunorubicin-treated samples (Fig. 2A and fig. S6A). By contrast, three of six missense mutants (R175H, R248Q, and R273H) lost nearly all DNA-binding activity. Two mutants (Y220C and M237I) had decreased but residual DNA-binding, with the target sites almost completely overlapping those found in cells with wild-type p53 and with no evidence for neomorphic binding sites (Fig. 2A and fig. S6, A to C). The R282W mutant had increased promoter occupancy, maintaining wild-type–like DNA-binding activity while also acquiring neomorphic binding sites (Fig. 2A and fig. S6, A to C).

Because promoter occupancy is necessary but not sufficient to transactivate expression of p53 target genes, we examined whether promoter binding of wild-type or mutant p53 results in expression of the associated genes (Fig. 2B and fig. S7, A to C). As expected, genes associated with wild-type–specific ChIP-seq peaks were expressed at higher levels in cells with wild-type *TP53* compared with cells with missense mutant or null alleles (Fig. 2B and fig. S7C). Even genes associated with ChIP-seq peaks shared between wild-type and missense mutant p53 were expressed at much higher levels in cells with wild-type *TP53* compared with cells with missense mutant or null alleles (Fig. 2B and fig. S7C). By contrast, genes associated with missense mutant–specific ChIP-seq peaks, most of which were contributed by R282W mutant, were not differentially expressed between cells with *TP53* missense mutant, null, or wild-type alleles (Fig. 2B and fig. S7C). These data indicate that p53 missense mutants are not capable of activating gene expression, including at de novo sites of p53 R282W mutant binding, even on exposure to chemotherapy.

To examine the possibility that missense mutant p53 drives an oncogenic GOF transcriptional program independent of its ability to directly act as a transcriptional activator or repressor, we analyzed our RNA-seq data without considering results from the ChIP-seq experiments. In contrast to previous reports that common p53 missense variants exert a universal transcriptional GOF (*14*, *15*), we found no indication of a common p53 missense mutant-driven GOF transcriptional program in either isogenic model, in steady state, or on daunorubicin-induced DNA damage (Fig. 2C and fig. S8, A to C). We did, however, identify a strong transcriptional signature

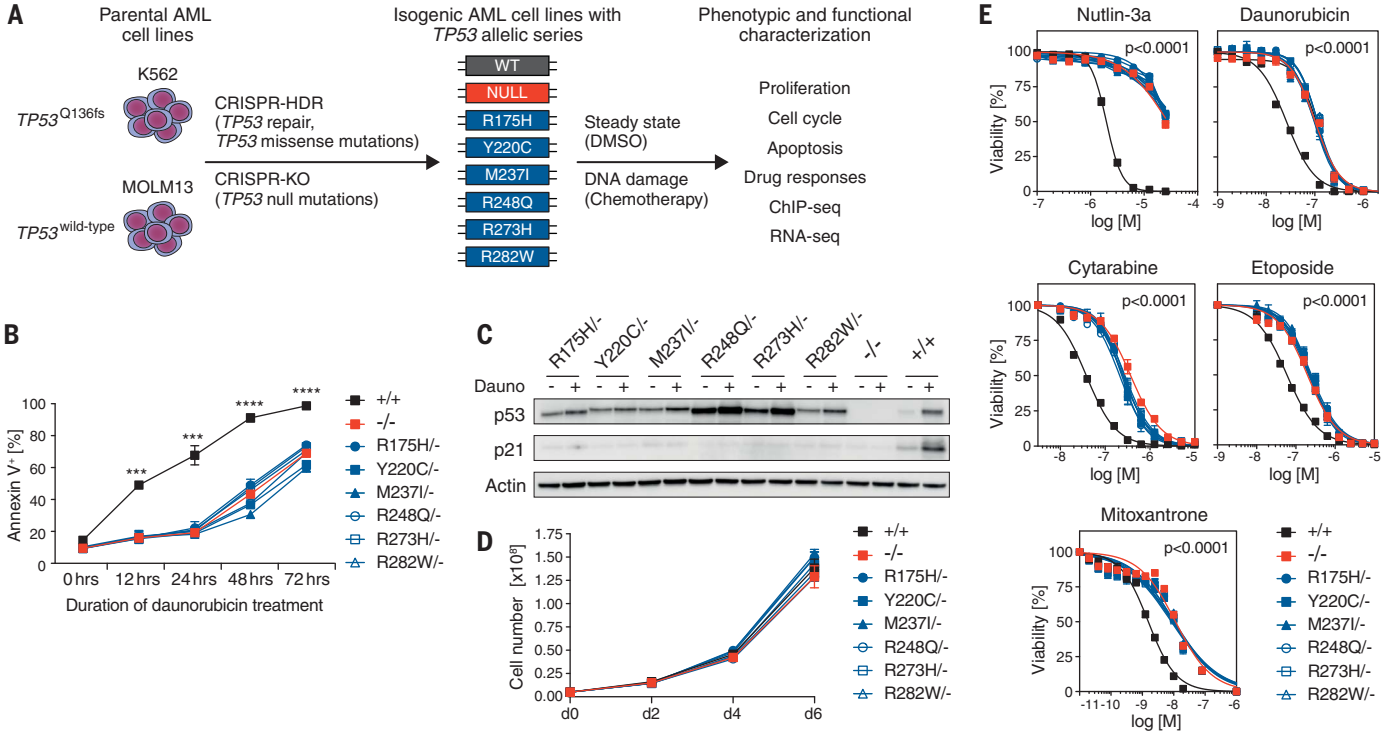

Fig. 1. *TP53* hotspot missense and null mutations in isogenic AML cell lines show similar oncogenic phenotypes. (**A**) Schematic of the experimental workflow for generating K562-*TP53* and MOLM13-*TP53* isogenic AML cell lines. CRISPR-HDR, CRISPR-Cas9–mediated homology-directed repair; CRISPR-KO, CRISPR-Cas9–mediated gene knockout; WT, wild-type. (**B**) MOLM13-*TP53* isogenic AML cell lines were treated with 100 nM daunorubicin for up to 72 hours. At the indicated time points, cells were stained with Annexin V and analyzed by flow cytometry to assess total apoptotic cells (replicates, $n = 3$; symbols represent averages of experimental replicates; error bars indicate SEM; ***$P < 0.001$, ****$P < 0.0001$, two-tailed Student's t test). (**C**) MOLM13-*TP53* isogenic AML cell lines were treated with DMSO (−) or 100 nM daunorubicin (+) for 6 hours, after which whole-cell protein lysates were collected, run on a polyacrylamide gel, and immunoblotted for p53, p21, and actin (replicates, $n = 3$; representative images are shown). Dauno, daunorubicin. (**D**) Growth kinetics of MOLM13-*TP53* isogenic AML cell lines (replicates, $n = 3$; symbols represent averages of experimental replicates; error bars indicate SEM). (**E**) MOLM13-*TP53* isogenic AML cell lines were treated with DMSO or indicated drugs at increasing concentrations for 72 hours, after which cell viability was assessed by using CellTiter-Glo luminescent assay (replicates, $n = 3$; symbols represent averages of experimental replicates; error bars indicate SEM). Single-letter abbreviations for the amino acid residues are as follows: C, Cys; H, His; I, Ile; M, Met; Q, Gln; R, Arg; W, Trp; and Y, Tyr.

of genes that have increased expression in *TP53* wild-type cells after DNA damage and that have lower expression in *TP53*-mutant cells. Notably, this signature was shared by all *TP53* missense and null mutant cells but not by *TP53* wild-type cells (Fig. 2C and fig. S8, A to C). This result emphasizes that the dominant gene expression signature of cells carrying *TP53* missense mutations is the signature of *TP53* inactivation, as demonstrated by equivalency to the transcriptional state of $TP53^{null}$ cells. Accordingly, gene ontology analysis performed on the 30 most differentially expressed genes revealed biological processes closely associated with p53-regulated pathways, such as apoptosis and cell cycle regulation, to be the most altered in cells with *TP53* missense mutant or null alleles (figs. S8D and S9, A and B).

As noted above, a DNE provides an alternative explanation to GOF mechanisms as a biological basis for the selective pressure for specific missense mutations (*16*–*19*). To test for DNE, we used CRISPR-Cas9 genome editing to generate isogenic MOLM13 cell lines with an allelic series that comprises $TP53^{+/+}$, $TP53^{+/-}$, $TP53^{-/-}$, $TP53^{R248Q/+}$, and $TP53^{R248Q/-}$. We used cyclin dependent kinase inhibitor 1A (*CDKN1A*) and p21 expression as a surrogate marker for p53 functionality. Daunorubicin treatment led to an increase in *CDKN1A* mRNA and p21 protein levels in $TP53^{+/+}$ and $TP53^{+/-}$ cells but not in $TP53^{-/-}$, $TP53^{R248Q/+}$, and $TP53^{R248Q/-}$ cells (Fig. 3A and fig. S10A). These results demonstrate that in heterozygous cells with endogenous expression of $p53^{R248Q}$ from one allele and endogenous $p53^{wild\text{-}type}$ from the other allele, the missense variant inhibits transcriptional activity of the wild-type p53 protein in a dominant-negative manner. Consequently, $TP53^{R248Q/+}$ cells showed a greater functional impairment of p53-dependent G_1 cell cycle arrest and apoptosis on daunorubicin treatment than $TP53^{+/-}$ cells did (Fig. 3B and fig. S10B). Moreover, $TP53^{-/-}$, $TP53^{R248Q/+}$, and $TP53^{R248Q/-}$ cells were functionally equivalent, as demonstrated by an equal degree of resistance to daunorubicin or nutlin-3a, an inhibitor of MDM2-mediated proteasomal degradation of p53, compared with $TP53^{+/+}$ and $TP53^{+/-}$ cells (Fig. 3C). Similarly, both $TP53^{R248Q/+}$ and $TP53^{R248Q/-}$ cells rapidly outcompeted $TP53^{+/+}$ cells in coculture assays in the presence of nutlin-3a (fig. S10C). Collectively, these data demonstrate that $p53^{R248Q}$ exerts a DNE on the functionality of $p53^{wild\text{-}type}$ in heterozygous AML cells, leading to enhanced competitive fitness of $TP53^{R248Q/+}$ compared with $TP53^{+/-}$ cells after DNA damage.

We next sought to examine all potential *TP53* missense mutations in an unbiased fashion. To this end, we performed a saturation mutagenesis screen in which each amino acid in p53 was systematically mutated to all other possible amino acids and a stop codon, as previously described (*24*). We introduced this pool of *TP53*-mutant cDNAs into a reporter AML cell line with wild-type p53 activity that was engineered to express a p21–green fluorescent protein (GFP) fusion protein from the endogenous *CDKN1A* locus. This enabled us to monitor by flow cytometry the biochemical consequences of p53 missense variants on wild-type p53's transcriptional activity (fig. S11, A and B). Reporter cells expressing the mutant cDNAs were treated with nutlin-3a to induce p53, and cells were sorted and sequenced on the basis of p21-GFP expression (fig. S11C). Amino acid substitutions at residues 100 to 300,

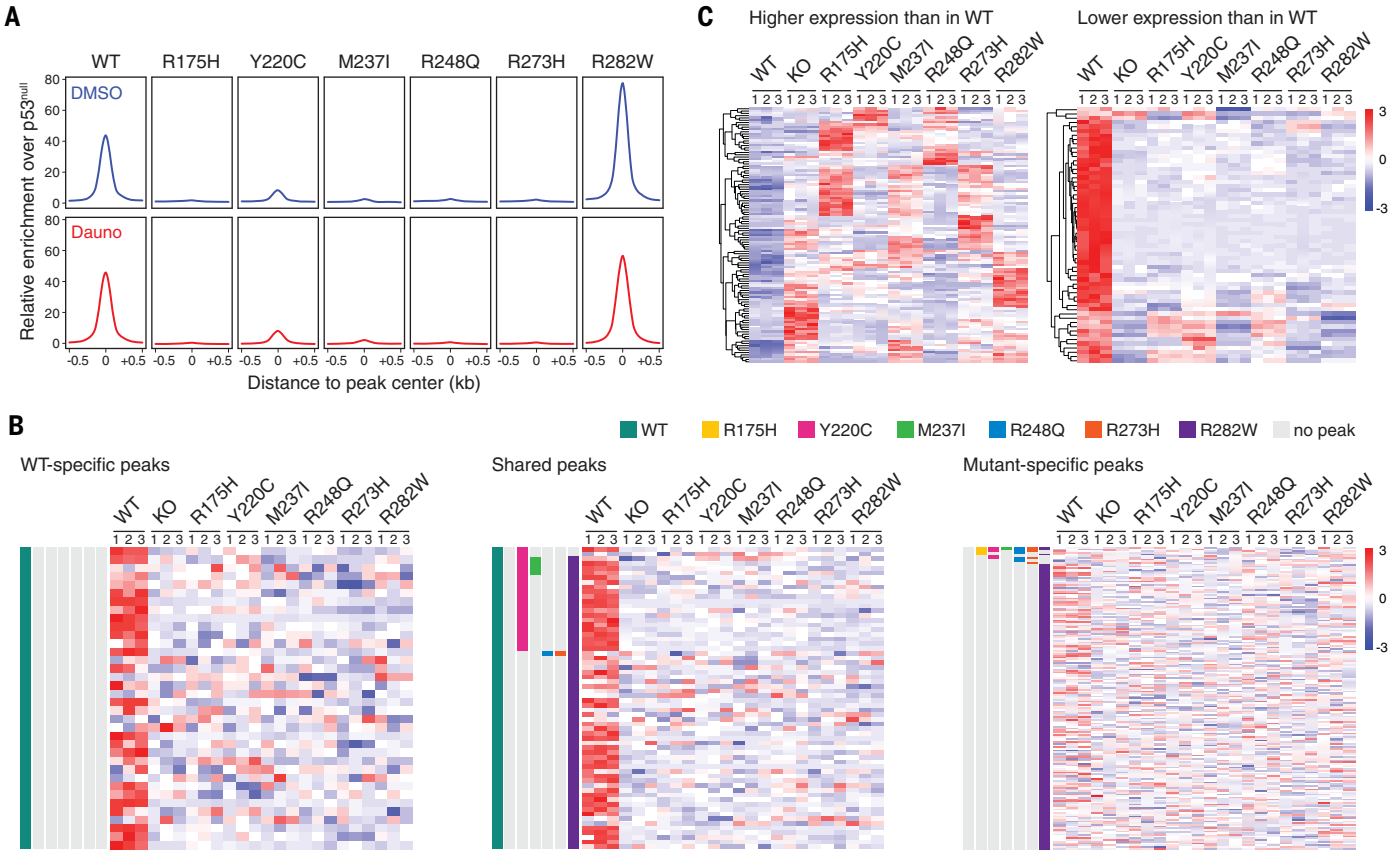

Fig. 2. Transcriptional consequences of *TP53* hotspot missense mutations in isogenic AML cell lines. (**A**) Genome-wide relative enrichment of wild-type and missense mutant p53 variants (ChIP for wild-type or missense mutant p53 over ChIP in $p53^{-/-}$ cells) over transcriptional start site–proximal regions (−10 kb to first intron) in K562-*TP53* isogenic cell lines on treatment with DMSO or 100 nM daunorubicin for 24 hours. (**B**) Heatmap depicting normalized expression of genes associated with WT-specific (left), shared (middle), and p53 mutant–specific (right) ChIP-seq peaks in K562-*TP53* isogenic cell lines treated with 100 nM daunorubicin for 24 hours (experimental replicates, $n = 3$). (**C**) Heatmap of the pooled top 30 (left) and pooled bottom 30 (right) genes relative to wild-type p53 in K562-*TP53* isogenic cell lines treated with 100 nM daunorubicin for 24 hours (RNA-seq experimental replicates, $n = 3$).

encompassing the DNA-binding domain, were powerfully enriched for dominant-negative activity both in DMSO- and nutlin-3a–treated reporter cells (Fig. 3D and fig. S11D). The amino acid substitutions resulting in DNE in our functional screen are highly concordant with missense *TP53* mutations in a cohort of 1040 patients with myeloid malignancies (Fig. 3D). Two saturation mutagenesis studies conducted in solid tumor models have recently reported conflicting results supportive of DNE (*24*) or loss-of-function and GOF effects (*25*). This discrepancy is most likely due to the lack of intrinsic wild-type p53 expression in the cell lines used by Kotler *et al.* (*25*) compared with those in our study. Collectively, our findings demonstrate that the vast majority of *TP53* missense mutations occurring in the DNA-binding domain, including those recurrently found in myeloid malignancies, exert a strong DNE on wild-type p53's transcriptional activity, whereas missense mutations outside of the DNA-binding domain have either loss-of-function or neutral effects.

Having studied the functional consequences of *TP53* missense mutations in isogenic AML cell line models in vitro, we sought to investigate the role of initiating *TP53* missense mutations on the response to DNA damage in hematopoietic stem and progenitor cells (HSPCs) in vivo. Preleukemic HSPCs carrying *TP53* mutations, including the missense mutations investigated in this study, undergo clonal selection after exposure to DNA-damaging chemotherapeutics (*26*), but the relative impact of specific *TP53* mutations is unknown. We generated mixed chimeric mice by transplanting HSPCs of various combinatorial genotypes derived from *Trp53* (gene nomenclature in mice is *Trp53* as opposed to *TP53* in humans) wild-type, *Trp53* knock-out, and *Trp53* knock-in mice expressing the mouse homologs of R175H (R172H in mice) and R273H (R270H in mice) (*10*). We followed peripheral blood chimerism in sublethally irradiated and control mice over time to determine the *Trp53* genotype-specific relative competitive fitness on DNA damage (Fig. 4A). As expected, $Trp53^{-/-}$ HSPCs had a strong competitive advantage over $Trp53^{+/+}$ or $Trp53^{+/-}$ HSPCs after sublethal irradiation, whereas $Trp53^{+/-}$ HSPCs expanded only modestly relative to $Trp53^{+/+}$ HSPCs (Fig. 4B). $Trp53^{+/+}$ HSPCs expressing congenic markers CD45.1 or CD45.2 had no competitive difference (Fig. 4B). The competitive advantage of $Trp53^{R172H/+}$ or $Trp53^{R270H/+}$ over $Trp53^{+/+}$ HSPCs

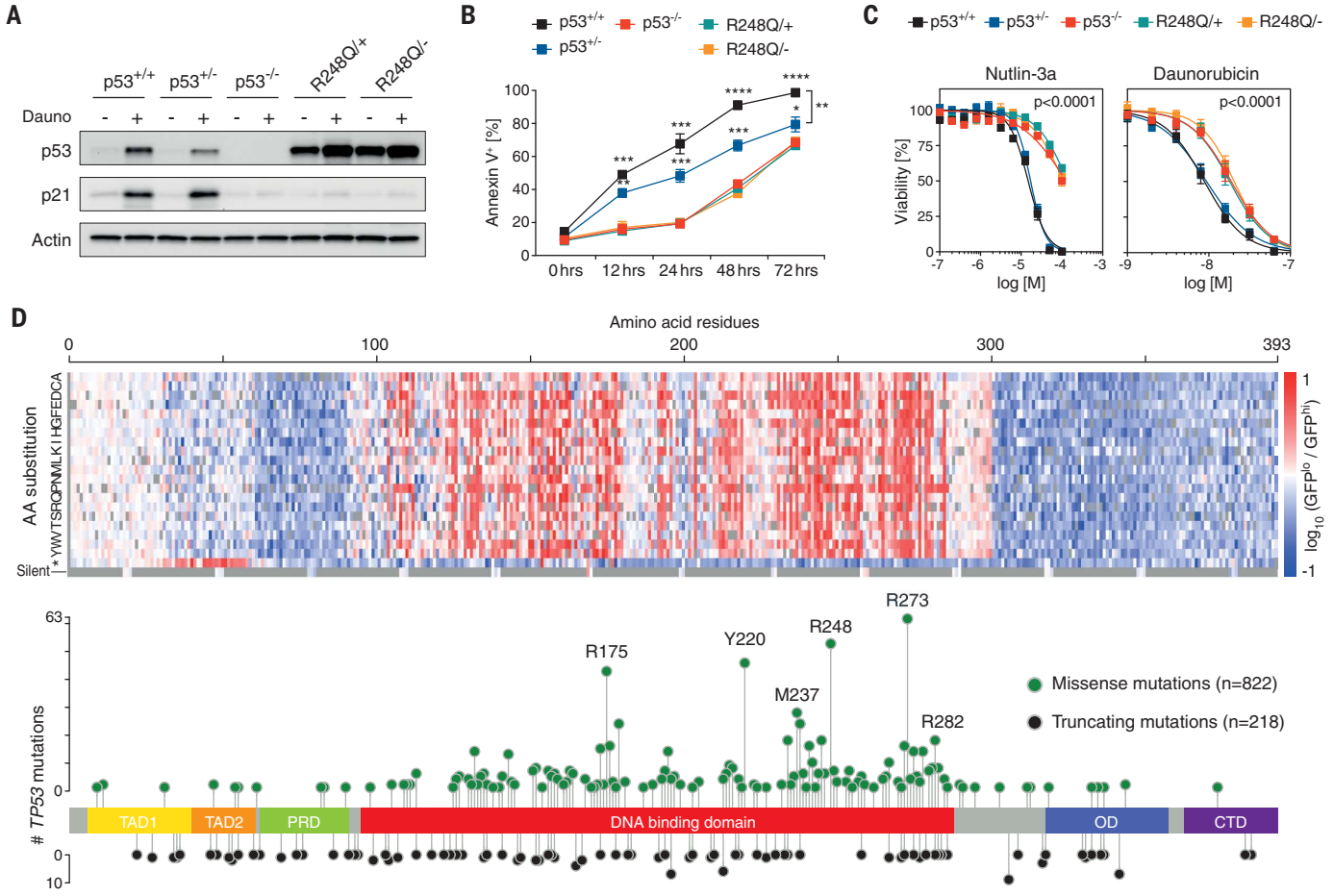

Fig. 3. *TP53* missense mutations in the DNA-binding domain confer a DNE. (**A**) MOLM13-*TP53* isogenic AML cell lines with $p53^{+/+}$, $p53^{+/-}$, and $p53^{-/-}$ as well as $p53^{R248Q/+}$ and $p53^{R248Q/-}$ were treated with DMSO (−) or 100 nM daunorubicin (+) for 6 hours, after which whole-cell protein lysates were collected, run on a polyacrylamide gel, and immunoblotted for p53, p21, and actin (replicates, $n = 3$; representative images are shown). (**B**) MOLM13-*TP53* isogenic AML cell lines were treated with 100 nM daunorubicin for up to 72 hours. At the indicated time points, cells were stained with Annexin V and analyzed by flow cytometry to assess total apoptotic cells (replicates, $n = 3$; symbols represent averages of experimental replicates; error bars indicate SEM; $*P = 0.05$, $**P = 0.01$, $***P < 0.001$, $****P < 0.0001$, two-tailed Student's t test). (**C**) MOLM13-*TP53* isogenic AML cell lines were treated with DMSO, nutlin-3a, or daunorubicin at increasing concentrations for 72 hours, after which cell viability was assessed by using CellTiter-Glo luminescent assay (replicates, $n = 3$; symbols represent averages of experimental replicates; error bars indicate SEM). (**D**) Heatmap depicting the *TP53* saturation mutagenesis screen results after nutlin-3a treatment, shown as $\log_{10}$ of the ratio of normalized read counts in GFP^{lo} over GFP^{hi} cells per *TP53* variant (top panel) overlaid on a lollipop plot demonstrating *TP53* mutational data from 1040 patients with MDS, myeloproliferative neoplasms, and AML (bottom panel). Missense mutations (green circles) and truncating mutations (black circles) comprising frame-shift, nonsense, and splice mutations are shown. AA, amino acid; CTD, C-terminal domain; OD, oligomerization domain; PRD, proline-rich domain; TAD, transactivation domain.

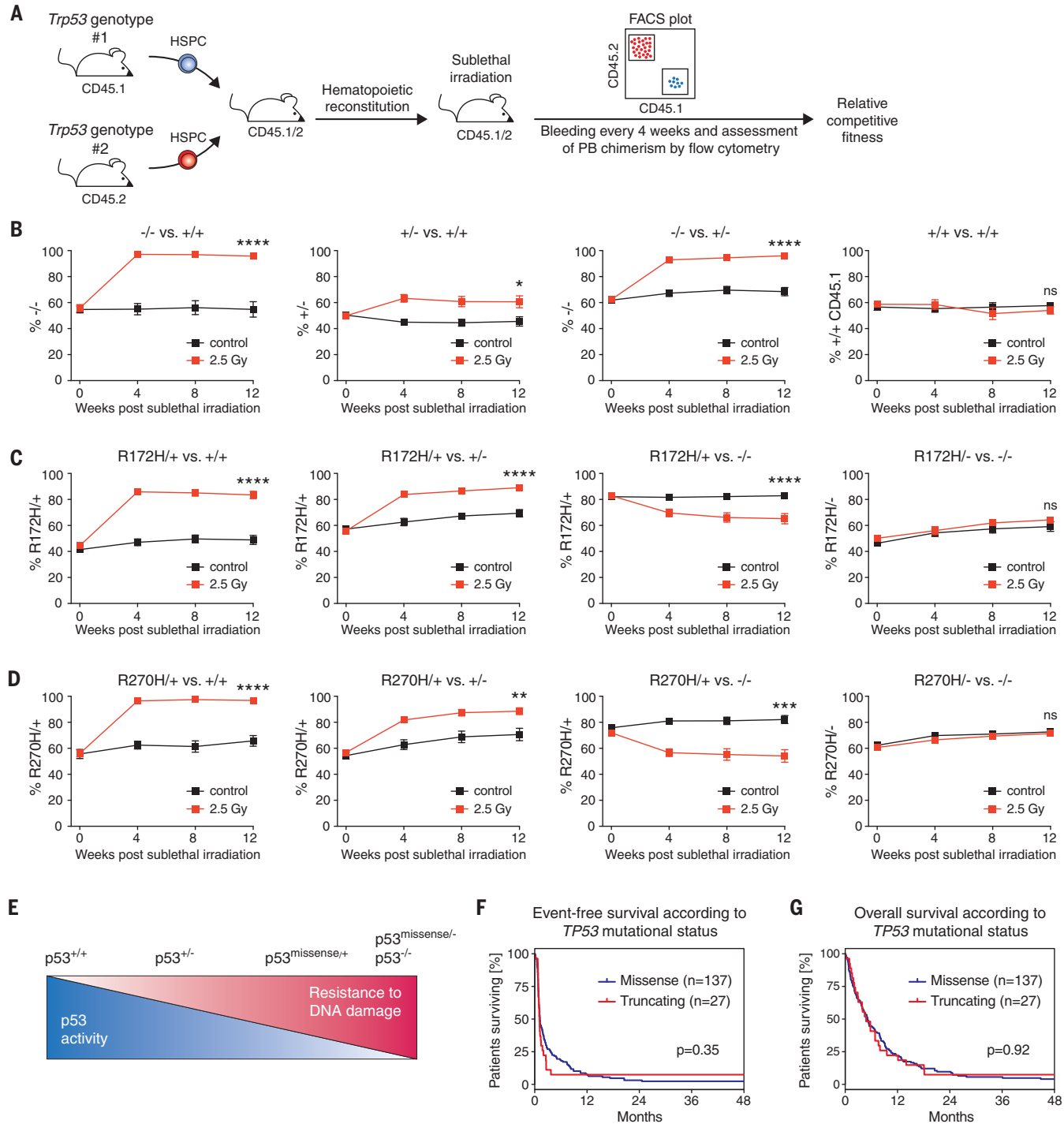

Fig. 4. Heterozygous *Trp53* missense mutations confer a competitive advantage over *Trp53*$^{+/-}$ HSPCs on sublethal gamma irradiation. (**A**) Schematic of the experimental workflow for hematopoietic competition assays in mixed chimeric mice to assess the relative competitive fitness of *Trp53* genotypes on sublethal gamma irradiation. *Trp53*$^{+/+}$-CD45.1/2 recipient mice were engrafted with a 1:1 mixture of *Trp53* genotypes from either CD45.1 or CD45.2 mice. After hematopoietic reconstitution, mixed chimeric mice were sublethally gamma-irradiated [single dose of 2.5 gray (Gy)], and thereafter, PB chimerism was assessed by flow cytometry every 4 weeks. FACS, fluorescent-activated cell sorting; PB, peripheral blood. (**B** to **D**) PB chimerism in mixed chimeric mice of the indicated genotypes in nonirradiated control mice (black squares) and mice treated with a single dose of 2.5 Gy gamma irradiation (red squares) (experimental replicates, n = 2 to 3 per group; n = 14 to 20 mice per group; symbols represent averages of individual mice across experimental replicates; error bars indicate SEM; *P < 0.05, **P < 0.01, ***P < 0.001, ****P < 0.0001, Mann-Whitney test). ns, not significant. (**E**) Schematic summary of the results obtained from hematopoietic competition assays depicting the relative competitive fitness of the indicated *Trp53* genotypes toward sublethal DNA damage. (**F**) Kaplan-Meier analysis for event-free and (**G**) overall survival in patients with AML according to *TP53* mutational status [missense mutations, blue line; truncating mutations comprising frame-shift, nonsense, and splice mutation, red line; log-rank (Mantel-Cox) test].

was similar in magnitude to the competitive advantage of $Trp53^{-/-}$ over $Trp53^{+/+}$ HSPCs (Fig. 4, B to D). $Trp53^{R172H/+}$ or $Trp53^{R270H/+}$ outcompeted $Trp53^{+/-}$ HSPCs (Fig. 4, C and D). By contrast, $Trp53^{R172H/-}$ or $Trp53^{R270H/-}$ HSPCs displayed no competitive advantage over $Trp53^{-/-}$ HSPCs (Fig. 4, C and D). These results demonstrate that these p53 missense variants exert a DNE on wild-type p53 on DNA damage, leading to expansion of HSPCs in vivo in mice. We noted slight increases in chimerism even in nonirradiated control mice. However, these reached plateaus and were therefore interpreted as posttransplant fluctuations. The results do not support a model in which the missense variants confer a GOF on p53 in mice. Intriguingly, $Trp53^{R172H/+}$ or $Trp53^{R270H/+}$ HSPCs had a competitive disadvantage relative to $Trp53^{-/-}$ HSPCs (Fig. 4, C and D), which reveals that the DNE is incomplete in vivo, leading to residual wild-type p53 activity. This finding is consistent with the ongoing selective pressure to inactivate the remaining wild-type allele in patients with heterozygous missense mutations (*6*). Collectively, the various possible configurations of *Trp53* alleles in biallelic HSPCs result in a graded decrease in p53 activity that is paralleled by an increased resistance to genotoxic stress (Fig. 4E).

To examine whether our results are consistent with clinical observations, we investigated the association of *TP53* mutation type on clinical outcomes in patients with AML. We analyzed a cohort of 164 patients with *TP53*-mutant AML from the German-Austrian AML Study Group who had received intensive, anthracycline-/cytarabine-based chemotherapy. Consistent with the well-known *TP53* mutational spectrum, the vast majority of patients (n = 137) had missense mutations, most of which (95.3%) were located in the DNA-binding domain (fig. S12A). A small number of patients (n = 27) had truncating mutations comprising frame-shift, nonsense, or splice mutations, and these mutations were evenly distributed across the gene (fig. S12A). An oncogenic p53 GOF in AML would be predicted to result in a more aggressive disease and worse survival outcomes in patients with missense mutations compared with patients who harbor truncating mutations. We found that patients with AML and missense mutations did not have a more aggressive disease than those with truncating mutations (fig. S12B) and observed no significant difference in event-free (P = 0.35) or overall (P = 0.92) survival in patients bearing *TP53* missense or truncating mutations (Fig. 4, F and G). In the subset of 101 patients (n = 87 missense mutations; n = 14 truncating mutations) for which co-mutation data were available (fig. S13A), we did not observe statistically significant differences in the number of co-mutations per patient. Co-mutations were present in 7 of 14 (50%) and 42 of 87 (48.3%) patients with AML and *TP53* truncating or missense mutations, respectively (P = 0.9999, Fisher's exact test). There was no evidence for a more aggressive co-mutational pattern in patients with AML and *TP53*, and the frequency of complex karyotype was not significantly different in patients with *TP53* missense mutations or truncating mutations. Overall, the outcomes of patients with AML and *TP53* mutations in this dataset do not support the hypothesis that a putative mutant p53-mediated GOF causes a worse outcome in patients with *TP53* missense mutations.

In aggregate, phenotypic and functional analyses in isogenic human AML cell line models, in vivo functional studies in mice, and analyses of clinicogenomic data from patients with AML consistently indicate that *TP53* missense mutations have dominant-negative activity without evidence of GOF capacity. We therefore propose a model in which missense variants exert a DNE that shapes the mutational spectrum early in the development of myeloid malignancies, often still at the premalignant stage (*27*–*30*), thereby providing a clonal reservoir of cells that are prone to expand and acquire secondary mutations, resulting in the development of myeloid malignancies. The concordance of the *TP53* mutational spectrum between premalignant clonal hematopoiesis of indeterminate potential and AML (fig. S12A) suggests no major selective pressures for specific *TP53* mutations during disease progression into AML. Similar observations have been made in studies comparing premalignant lesions and overt cancer of the skin and esophagus (*31*, *32*). Notably, the nearly identical *TP53* mutational spectrum in myeloid malignancies and solid tumors strongly suggest similar selection processes in many if not most cancers. Previous studies have demonstrated mutant p53 GOF mechanisms in epithelial cancers, implicating neomorphic protein-protein interactions with other transcription factors, including p63, NF-Y, NRF2, and ETS2 (*11*, *14*, *15*, *33*). The discrepancy between our study and previous studies may be explained by distinct expression levels of these transcription factors in epithelial compared with those in hematopoietic cells. For p63, a p53 family member, variable expression, predominantly in epithelial tissues, has indeed been reported (*34*), suggesting that GOF may be context dependent (*35*).

Our studies demonstrate that in myeloid malignancies, *TP53* missense mutations do not lead to neomorphic GOF activities but instead drive clonal selection through a DNE. Future studies aimed at elucidating the molecular mechanisms of the DNE may lead to therapeutic strategies that prevent outgrowth of *TP53*-mutant clones and progression into AML and MDS.

REFERENCES AND NOTES

1. A. J. Levine, M. Oren, *Nat. Rev. Cancer* **9**, 749–758 (2009).
2. R. Bejar *et al.*, *N. Engl. J. Med.* **364**, 2496–2506 (2011).
3. F. G. Rücker *et al.*, *Blood* **119**, 2114–2121 (2012).
4. R. C. Lindsley *et al.*, *N. Engl. J. Med.* **376**, 536–547 (2017).
5. E. R. Kastenhuber, S. W. Lowe, *Cell* **170**, 1062–1078 (2017).
6. Y. Liu *et al.*, *Nature* **531**, 471–475 (2016).
7. R. Brosh, V. Rotter, *Nat. Rev. Cancer* **9**, 701–713 (2009).
8. E. H. Baugh, H. Ke, A. J. Levine, R. A. Bonneau, C. S. Chan, *Cell Death Differ.* **25**, 154–160 (2018).
9. D. Dittmer *et al.*, *Nat. Genet.* **4**, 42–46 (1993).
10. K. P. Olive *et al.*, *Cell* **119**, 847–860 (2004).
11. S. Di Agostino *et al.*, *Cancer Cell* **10**, 191–202 (2006).
12. P. M. Do *et al.*, *Genes Dev.* **26**, 830–845 (2012).
13. J. Xu *et al.*, *Nat. Chem. Biol.* **7**, 285–295 (2011).
14. J. Zhu *et al.*, *Nature* **525**, 206–211 (2015).
15. D. Walerych *et al.*, *Nat. Cell Biol.* **18**, 897–909 (2016).
16. S. Srivastava, S. Wang, Y. A. Tong, Z. M. Hao, E. H. Chang, *Cancer Res.* **53**, 4452–4455 (1993).
17. M. E. Hegi *et al.*, *Cancer Res.* **60**, 3019–3024 (2000).
18. A. de Vries *et al.*, *Proc. Natl. Acad. Sci. U.S.A.* **99**, 2948–2953 (2002).
19. M. K. Lee *et al.*, *Cancer Cell* **22**, 751–764 (2012).
20. A. J. McGahon *et al.*, *Cell Death Differ.* **4**, 95–104 (1997).
21. K. Chylicki *et al.*, *Cell Growth Differ.* **11**, 315–324 (2000).
22. A. M. A. Di Bacco, T. G. Cotter, *Br. J. Haematol.* **117**, 588–597 (2002).
23. S. J. Baker, S. Markowitz, E. R. Fearon, J. K. Willson, B. Vogelstein, *Science* **249**, 912–915 (1990).
24. A. O. Giacomelli *et al.*, *Nat. Genet.* **50**, 1381–1387 (2018).
25. E. Kotler *et al.*, *Mol. Cell* **71**, 178–190.e8 (2018).
26. T. N. Wong *et al.*, *Nature* **518**, 552–555 (2015).
27. S. Jaiswal *et al.*, *N. Engl. J. Med.* **371**, 2488–2498 (2014).
28. G. Genovese *et al.*, *N. Engl. J. Med.* **371**, 2477–2487 (2014).
29. S. Abelson *et al.*, *Nature* **559**, 400–404 (2018).
30. P. Desai *et al.*, *Nat. Med.* **24**, 1015–1023 (2018).
31. I. Martincorena *et al.*, *Science* **348**, 880–886 (2015).
32. I. Martincorena *et al.*, *Science* **362**, 911–917 (2018).
33. M. Adorno *et al.*, *Cell* **137**, 87–98 (2009).
34. C. J. Di Como *et al.*, *Clin. Cancer Res.* **8**, 494–501 (2002).
35. M. P. Kim, G. Lozano, *Cell Death Differ.* **25**, 161–168 (2018).

ACKNOWLEDGMENTS

We thank A. S. Sperling, R. S. Sellar, and M. Slabicki for their critical review of the manuscript. **Funding:** B.L.E. and S.A.A. received funding from the NIH (P01CA066996, P50CA206963, and R01HL082945). B.L.E was funded by the Howard Hughes Medical Institute, the Edward P. Evans Foundation, the Leukemia and Lymphoma Society, the Adelson Medical Research Foundation, and the Henry and Marilyn Taub Foundation. S.B. was supported by fellowships from the Swiss Cancer League (KLS-3625-02 2015) and Swiss National Science Foundation (P300PB_161026/1 and P400PM_183862). K.J.K was supported by the Jane and Aatos Erkko Foundation, Orion Research Foundation, and Instrumentarium Science Foundation. This work was supported in part by grants U01 CA176058 (W.C.H.) and U01 CA199253 (W.C.H. and T.J.). **Author contributions:** S.B. devised and conducted experiments and wrote the manuscript. P.G.M., R.S., M.M., M.L., W.W., J.K., S.C., K.J.K., R.C.L., P.A.J., and T.J. helped with experiments, provided reagents, and analyzed data. A.O.G., W.C.H., X.Y., K.M., F.P., and D.E.R. helped perform and analyze the *TP53* saturation mutagenesis screen. A.V.K. and S.A.A. helped perform and analyze ChIP-seq and RNA-seq analyses. H.D. and F.G.R. provided *TP53* mutational and clinical data, and Y.F. and D.N. analyzed *TP53* mutational and clinical data from patients with AML. B.L.E. directed the study and wrote the manuscript. All authors contributed to writing of the manuscript. **Competing interests:** P.G.M. receives consulting fees from Foundation Medicine, Inc. W.C.H. is a consultant for ThermoFisher, Parexel, AjuIB, and MPM and is a founder of and adviser to KSQ Therapeutics. S.A.A. has been a consultant and/or shareholder for Epizyme, Inc.; Imago Biosciences; Cyteir Therapeutics; C4 Therapeutics; Syros Pharmaceuticals; OxStem Oncology; Accent Therapeutics; and Mana Therapeutics. S.A.A. has received research support from Janssen, Novartis, and AstraZeneca. B.L.E. has been a consultant for Grail and has received research support from Celgene and Deerfield. **Data and materials availability:** ChIP-seq and RNA-seq data are being made accessible at the Gene Expression Omnibus database repository GSE131484 (ChIP-seq) and GSE131592 (RNA-seq). Materials are available from B.L.E. on request.

SUPPLEMENTARY MATERIALS

science.sciencemag.org/content/365/6453/599/suppl/DC1
Materials and Methods
Figs. S1 to S13
Tables S1 and S2
References (*36*–*55*)

17 March 2019; accepted 24 June 2019
10.1126/science.aax3649

A dominant-negative effect drives selection of *TP53* missense mutations in myeloid malignancies

Steffen Boettcher, Peter G. Miller, Rohan Sharma, Marie McConkey, Matthew Leventhal, Andrei V. Krivtsov, Andrew O. Giacomelli, Waihay Wong, Jesi Kim, Sherry Chao, Kari J. Kurppa, Xiaoping Yang, Kirsten Milenkowic, Federica Piccioni, David E. Root, Frank G. Rücker, Yael Flamand, Donna Neuberg, R. Coleman Lindsley, Pasi A. Jänne, William C. Hahn, Tyler Jacks, Hartmut Döhner, Scott A. Armstrong and Benjamin L. Ebert

Science **365** (6453), 599-604.
DOI: 10.1126/science.aax3649

p53—still hazy after all these years?

The gene encoding the p53 tumor suppressor protein is the most frequently mutated gene in human cancer. Yet decades after the gene's discovery, the biology of cancer-associated missense mutations in p53 is still being debated. Previous studies have suggested that missense mutations confer tumor-promoting functions to p53. Boettcher *et al.* conducted a detailed analysis of p53 missense mutations in human leukemia, drawing on methodologies including genome editing, a p53 saturation mutagenesis screen, mouse models, and clinical data (see the Perspective by Lane). They found no evidence that p53 missense mutations confer an oncogenic gain of function. Rather, the mutations exerted a dominant-negative effect that reduced the tumor suppressor activity of wild-type p53.

Science, this issue p. 599; see also p. 539